Nanoscale magnetic sensing using spin qubits in diamond

Citation: Maze, J. R. et al. "Nanoscale magnetic sensing using spin qubits in diamond." Advanced Optical Concepts in Quantum Computing, Memory, and Communication II. Ed. Zameer U. Hasan, Alan E. Craig, & Philip R. Hemmer. San Jose, CA, USA: SPIE, 2009. 722509-8. © 2009 SPIE

As Published: http://dx.doi.org/10.1117/12.813802

Publisher: Society of Photo-optical Instrumentation Engineers

Persistent URL: http://hdl.handle.net/1721.1/52648

Version: Final published version: final published article, as it appeared in a journal, conference proceedings, or other formally published context

Invited Paper

Nanoscale magnetic sensing using spin qubits in diamond

J.R. Maze[1], P. Cappellaro[1,2], L. Childress[3], M.V.G. Dutt[4], J.S. Hodges[1,5], S. Hong[1], L. Jiang[1], P.L. Stanwix[2], J.M. Taylor[6], E. Togan[1], A.S. Zibrov[1], P. Hemmer[7], A. Yacoby[1], R.L. Walsworth[1,2] and M. D. Lukin[1]

[1] Department of Physics, Harvard University, Cambridge, MA 02138 USA.
[2] Harvard-Smithsonian Center for Astrophysics, Cambridge, MA 02138 USA.
[3] Department of Physics, Bates College, Lewiston, ME 04240 USA.
[4] Department of Physics and Astronomy, University of Pittsburgh, Pittsburgh, PA 15260, USA.
[5] Department of Nuclear Science and Engineering, [6] Department of Physics, Massachusetts Institute of Technology, Cambridge, MA 02139 USA.
[7] Department of Electrical and Computer Engineering, Texas A&M University, College Station, TX 77843 USA.

ABSTRACT

The ability to sense nanotelsa magnetic fields with nanoscale spatial resolution is an outstanding technical challenge relevant to the physical and biological sciences. For example, detection of such weak localized fields will enable sensing of magnetic resonance signals from individual electron or nuclear spins in complex biological molecules and the readout of classical or quantum bits of information encoded in an electron or nuclear spin memory. Here we present a novel approach to nanoscale magnetic sensing based on coherent control of an individual electronic spin contained in the Nitrogen-Vacancy (NV) center in diamond. At room temperature, using an ultra-pure diamond sample, we achieve shot-noise-limited detection of 3 nanotesla magnetic fields oscillating at kHz frequencies after 100 seconds of signal averaging. Furthermore, we experimentally demonstrate nanoscale resolution using a diamond nanocrystal of 30 nm diameter for which we achieve a sensitivity of 0.5 microtesla / $\mathrm{Hz}^{1/2}$.

Keywords: Quantum control, solid-state qubits, magnetometry.

1. INTRODUCTION

Detection of weak magnetic fields has historically been achieved using atomic/molecular systems or solid-state devices with distinctly different underlying physics. Precision measurement techniques in atomic and molecular systems,[1,2] widely used to implement ultra-stable atomic clocks,[3–5] rely on monitoring the precession of angular momentum via the Zeeman effect for magnetic field sensing.[6,7] Sensitive solid-state magnetometers are generally based on many-body macroscopic phenomena such as the Josephson effect in SQUIDs[8,9] or the Hall effect in semiconductors.[10] Nevertheless, the state-of-the-art magnetometers achieve very high sensitivities, they have difficulty detecting weak fields with high spatial resolution. Of particular interest would be the detection and localization of the magnetic field produced by a single electronic or nuclear spin. Some intriguing techniques –such as magnetic force microscopy[11,12]– could potentially yield better spatial resolution. Here we investigate a novel approach to the detection of weak magnetic fields using systems currently explored as qubits: isolated electronic spins in diamond.[13–15] The present approach to magnetic sensing[16–18] combines the coherent manipulation of individual electronic spin qubits embedded in a solid-state environment with optical read-out, to yield an unprecedented combination of high sensitivity and spatial resolution.

Advanced Optical Concepts in Quantum Computing, Memory, and Communication II, edited by Zameer U. Hasan, Alan E. Craig, Philip R. Hemmer, Proc. of SPIE Vol. 7225, 722509 · © 2009 SPIE · CCC code: 0277-786X/09/$18 · doi: 10.1117/12.813802

2. SINGLE SPIN BASED MAGNETOMETRY

Figure 1-a illustrates the relevant level structure of the NV center in diamond. The center can be polarized via optical pumping and measured through spin state-selective fluorescence. Conventional ESR techniques are used to coherently manipulate the spin angular momentum via microwave fields. To achieve magnetic sensing, we monitor the electronic spin precession, which depends on external magnetic fields through the Zeeman effect. This method is directly analogous to precision magnetometry techniques in atomic and molecular systems.

The maximum sensitivity will ultimately be determined by the spin coherence time and spin projection-noise. Although solid-state electronic spins have shorter coherence times than gaseous atoms, quantum control techniques can decouple them from the local environment, leading to a substantial improvement in their sensitivity

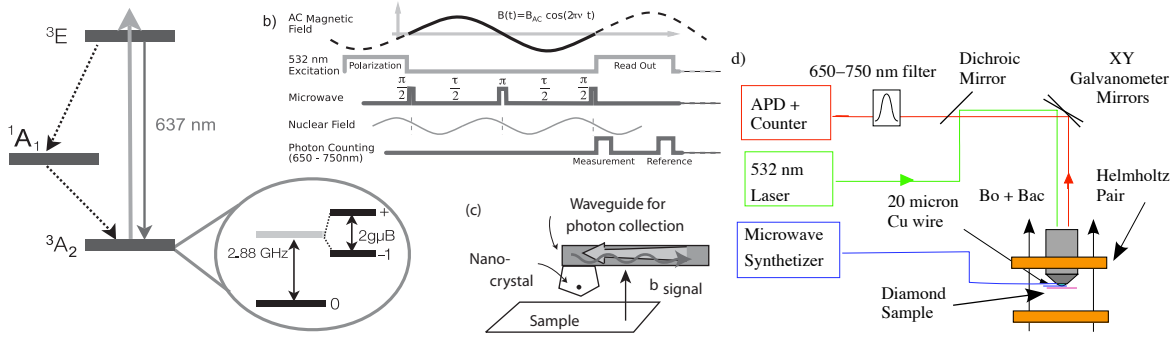

Figure 1. Principles of the individual NV electronic spin diamond magnetic sensor. (a) Energy levels for a single NV impurity. (b) Example of the pulse sequence structure of the experimental approach. (c) Scanning tip setup for high-spatial resolution magnetometry. (d) Experimental setup.

to external, time-varying magnetic fields. Although the sensitivity is smaller than that of the state-of-the-art macroscopic magnetometers, a key feature of our sensor is that it can be localized within a region of about 10 nm, either in direct proximity to a diamond surface or within a nano-sized diamond crystal, yielding high spatial resolution.

Figure 2-b describes our procedure to detect magnetic fields. The canonical approach consist on detecting Zeeman shifts by means of Ramsey-type spectroscopy. A $\pi/2$-pulse creates a superposition of two Zeeman levels, which acquire a relative phase $\phi = \delta\omega\ \tau \propto \frac{g\mu_B}{\hbar} B\tau$ from the external field B during the free evolution interval τ (here μ_B is the Bohr magneton and $g \approx 2$ for NV centers). Another $\pi/2$-pulse transforms the relative phase into a population difference, which is measured optically. For small ϕ, the magnetometer signal $\mathcal{S}$ (proportional to the induced population difference) depends linearly on the magnetic field: $\mathcal{S} \approx \frac{g\mu_B}{\hbar} B\tau$. During the total averaging interval T, T/τ measurements can be made, yielding a shot-noise-limited sensitivity δB given by the minimum detectable field, $B_{min} \equiv \delta B/\sqrt{T} = \frac{\hbar}{g\mu_B} \frac{1}{\sqrt{\tau T}}$.

As the interrogation time τ increases, the sensitivity improves until interactions with the environment lead to signal decay. For solid-state spin systems, the coherence is limited by interactions with nearby lattice nuclei and paramagnetic impurities, resulting in an ensemble dephasing time $T_2^* \sim 1\ \mu$s. However, coherent control techniques can improve the sensitivity for AC fields. Due to the long correlation times characteristic of dipolar interactions between nuclear spins —the principal source of dephasing— spin echo techniques can dramatically extend the coherence time. In particular, this can be achieved by adding an additional microwave π-pulse to the Ramsey sequence at time $\tau/2$, the Hahn echo sequence[19] removes the effect of environmental perturbations whose correlation time is long compared to τ. Thus a signal field $B(t)$ oscillating in-phase with the pulse sequence produces an overall additive phase shift, leading to a total phase accumulation, $\delta\phi = \frac{g\mu_B}{\hbar}[\int_0^{\tau/2} B(t)dt - \int_{\tau/2}^{\tau} B(t)dt]$. Correspondently, the probability of the spin being in the $m_s = 0$ state at the end of the sequence is $P_0(\tau) = [1 + F(\tau)\cos(\delta\phi)]/2$, where $F(\tau)$ is the amplitude of the spin-echo signal envelope in the absence of a time varying field (see Fig. 2-b). For maximal response to CW signals $B_{AC}\sin(\nu t + \varphi_0)$ with known frequency

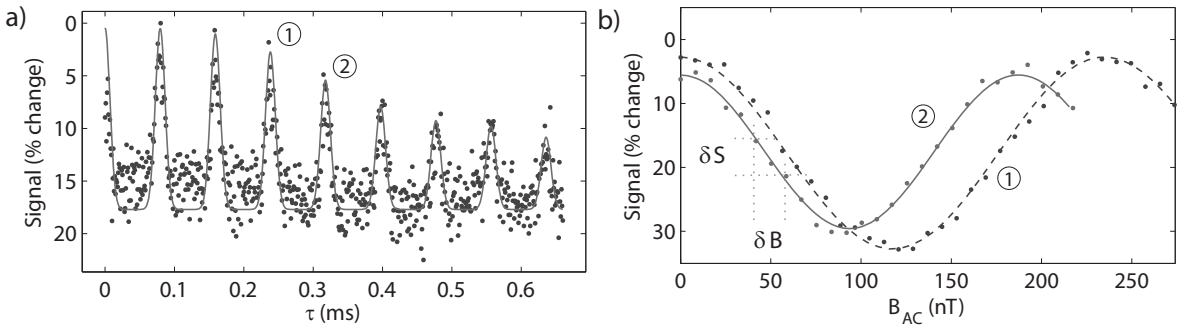

Figure 2. Spin-echo-based magnetometry with an individual NV electronic spin in a bulk diamond sample. (a) Example electronic spin-echo measurement (dots) and fitting (solid line, see text). (b) Spin-echo signal as a function of applied AC magnetic field amplitude for two operating frequencies $\nu_1 = 3.15$ kHz (dashed line) and $\nu_2 = 4.21$ kHz, corresponding to revivals 1 and 2 in Fig. 2-a.

and phase (assuming small B_{AC}), we find $\tau = 2\pi/\nu$ and $\varphi_0 = 0$ to be optimal. The resulting sensitivity per averaging time is

$$\delta B_{AC} \sim \frac{\pi\hbar}{2g\mu_B C\sqrt{T_2}}, \tag{1}$$

where $C \leq 1$, is a parameter that incorporates photon shot noise and a finite contrast to the Ramsey fringes.

An optimum sensitivity is achieved for fields with frequency close to $\nu \sim 1/T_2$. ensitivity can be improved for higher frequency signals by using composite pulse sequences such as CPMG[20] that may provide an even longer coherence time at the expense of a reduced bandwidth.

3. MAGNETIC SENSING USING NITROGEN-VACANCY CENTERS

3.1. Regimes of operation and achievable sensitivity

We implement magnetic sensing using single NV centers in diamond. The ground state for this center is a electronic spin triplet (shown in Fig. 1-a). The crystal field splits the $m_s = \pm 1$ Zeeman sublevels from the $m_s = 0$ sublevel by $\Delta = 2\pi \times 2.87$ GHz, setting the spin quantization axis along the nitrogen-vacancy line. There are two possible regimes of operations for the magnetometer, each providing a different compromise between the ease of control and achievable sensitivity.

For low static magnetic fields $B_{DC} \leq 10$ mT, it is preferable to use the $m_s = \pm 1$ manifold which provides a better sensitivity. It has twice the energy splitting of the 0-1 manifold and is less affected by nuclear spin-induced decoherence at low fields, since inter-nuclear interactions are suppressed by the large hyperfine field.[21] For diamond where natural abundance (1.1%) of Carbon-13 nuclei is the principal cause of decoherence, the signal decays as $F(\tau) = \exp[-(\tau/T_2)^3]$ with $T_2 \sim 300\mu$s.[22] We can optimize the sensitivity as a function of τ, $\delta B_{AC} = \frac{\pi\hbar}{2g\mu_B} e^{(\tau/T_2)^3}\sqrt{\tau + t_m}/C\tau$, to obtain a sensitivity of $\delta B_{AC} \approx 18$ nT Hz$^{-1/2}$ for a single NV center under current experimental conditions ($C \approx 0.05$ and measurement time $t_m \leq 2$ μs). Improved collection efficiencies ($C = 0.3$) would yield $\delta B_{AC} = 3$ nT/Hz$^{-1/2}$.

At high magnetic fields, it is convenient to address the $m_s = \{0, 1\}$ manifold. The dynamics imposed on the electronic spin by the nuclear spin bath is however more complex. Figure 2-a shows a typical spin-echo signal observed from an individual NV center. The periodic modulation of the echo is caused by a bath of ^{13}C nuclear spins, which create an effective precessing magnetic field of a few microtesla at the NV center. The precession of the nuclear spins around B_{DC} causes the NV spin-echo signal to collapse and revive[15] at half the rate of the ^{13}C Larmor frequency, $\omega_L = \gamma_{^{13}C} B_{DC}$. Note that substantial spin-echo revivals exist even after a free evolution of 0.6 ms. The decay of the echo signal envelope does not follow a simple exponential decay associated with typical ESR on bulk samples. This can be understood by noting that echo dynamics of a single NV center near the revivals is likely determined by a few ^{13}C that interacts strongly with the electronic spin,[13–15, 22, 23] yielding multiple characteristic time scales for the echo decay. The envelope of the spin echo signal in Figure 2-a has been

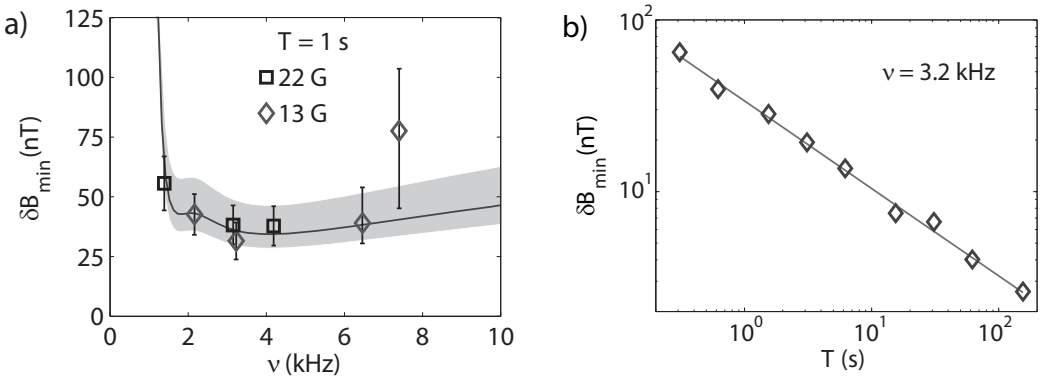

Figure 3. Magnetometer sensitivity characterization. (a) Measured sensitivity of a single NV spin magnetometer in bulk diamond after one second averaging. Error bars represent standard deviation for a sample size of 30. Also shown is the theoretically predicted sensitivity (solid line), with the shaded region representing uncertainty due to variations in photon collection efficiency. Measurements were carried out at two DC fields, $B_{DC} = 13$ (diamond) and 22 G (square). (b) Minimum measurable AC magnetic field as a function of averaging time, for AC field frequency $\nu = 3.2$ kHz and $B_{DC} = 13$ G (diamonds). Fit to the data shows that the sensitivity improves as the square root of averaging time, in agreement with theoretical estimates based on photon shot-noise limited detection.

modeled with an exponential decay $F(\tau) \propto \exp(-(\tau/T_2)^4)$ modulated by a pair of strongly interacting ^{13}C. The sensitivity is then

$$\delta B_{AC} = \frac{\pi\hbar}{g\mu_B} F(\tau)\sqrt{\tau + t_m}/C\tau. \quad (2)$$

With $T_2 \sim 600$ μs, the predicted optimal sensitivity is $\delta B_{AC} \approx 4$ nT/Hz$^{-1/2}$ for an ideal spin readout, while we expect a sensitivity $\gtrsim 25$ nT/Hz$^{-1/2}$ with current collection efficiencies, corresponding to $C \sim 0.05$.

3.2. First proof of principles realization

In order to establish the sensitivity limits of our magnetometer, we performed a series of proof-of-principle experiments involving single NV centers in bulk ultra-pure single crystal diamond and in commercially available diamond nanocrystals. Our experimental methodology is depicted in Figure 1. Single NV centers are imaged and localized with ~ 170 nm resolution using confocal microscopy. The position of the focal point is moved near the sample surface using a galvanometer mounted mirror to change the beam path and a piezo-driven objective mount. A 20 micron diameter wire generates microwave pulses to manipulate the electronic spin states (see Figure 1b). A pair of Helmholtz coils are used to provide both AC and DC magnetic fields. An individual center is first polarized into the $m_S = 0$ sublevel. On Figure 1-b, a coherent superposition between the states $m_S = 0$ and $m_S = 1$ is created by applying a $\pi/2$ pulse tuned to this transition. The system freely evolves for a period of time $\tau/2$, followed by a π refocusing pulse. After a second $\tau/2$ evolution period, the electronic spin state is projected onto the $m_S = \{0, 1\}$ basis by a final $\pi/2$ pulse, at which point the ground state population is detected optically via spin-dependent fluorescence.

First, we consider a single crystal diamond bulk sample, operating in the $m_s = \{0, 1\}$ manifold. To achieve the highest sensitivity, the revival rate of the spin-echo signal is adjusted by varying the strength of the applied DC magnetic field B_{DC}, such that the frequency of the echo revival peaks coincides with multiples of the AC field frequency ν to be detected. As shown in Figure 2-b, the observed peak of the spin-echo signal varies periodically as the amplitude of the external AC field (B_{AC}) is increased. The signal variation results from the accumulated phase due to the AC magnetic field, which is converted into a spin population difference, leading to variations in the detected fluorescence signal. Maximal signal on Figure 2 corresponds to an average number of photons $\bar{n} = 0.03$ detected during the 324 ns photon counting window of a single experimental run. On Figure 2-b, each displayed point is a result of $N = 7 \times 10^5$ averages of spin-echo sequences. The magnetometer is most sensitive to variations in the AC magnetic field amplitude (δB) at the point of maximum slope, with the sensitivity being limited by the uncertainty in the spin-echo signal measurement (δS).

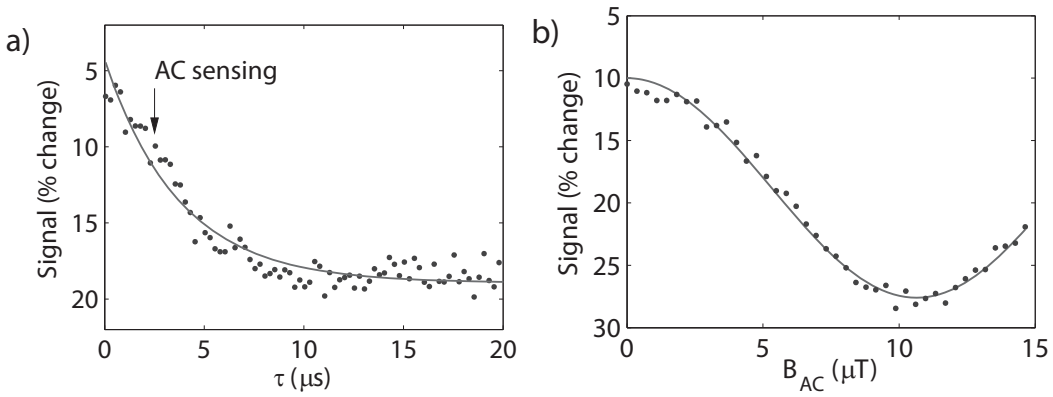

Figure 4. Example of magnetic sensing with a single NV electronic spin in a diamond nanocrystal. (a) Spin-echo signal from a single NV center contained in a diamond nanocrystal with diameter of 34±12 nm as determined by AFM. The arrow indicates the time at which magnetic sensing is performed in Fig. 4b. (b) Spin-echo signal as a function of the applied AC magnetic field amplitude at a frequency of $\nu = 380$ kHz. The resulting standard deviation yields a magnetometer sensitivity of 0.5 ± 0.1 μT/Hz$^{1/2}$.

Figure 3a shows a demonstration of the measured sensitivity δB after one second of averaging as a function of the AC magnetic field frequency $\nu = 1/\tau$. At high frequencies or short times, $F(1/\nu) \to 1$, and the sensitivity scales as $\sqrt{\nu}$, while at low frequencies decoherence degrades the sensitivity. Figure 3-b shows sensitivity for a fixed AC magnetic field frequency ν as a function of measurement time T. The solid line is a fit to $B_{min} \propto T^{-\alpha}$, where $\alpha = 0.5 \pm 0.01$. This indicates that magnetic fields as small as few nanotesla are resolvable after 100 seconds of averaging.

In addition, we performed similar experiments using single NV centers in diamond nanocrystals (30 nm diameter) to demonstrate magnetic sensing within a nanoscale detection volume. The available nanocrystals contain a large number of impurities (probably paramagnetic substitutional nitrogen atoms containing unpaired electron spins) that shorten the electronic spin coherence time[24] to values ranging from 4 to 10 μs. Sensitive detection of AC magnetic fields is still possible as demonstrated experimentally in Figure 4. A magnetometer sensitivity of $\delta B \sim 0.5 \pm 0.1$ $\mu\text{T}/\sqrt{Hz}$ is achieved for this nanocrystal at $\nu = 380$ kHz. In Figure 4-b, maximum signal corresponds to an average number of photons $\bar{n} = 0.02$ counted during a 324 ns photon counting window; $N = 2 \times 10^6$ averages of spin-echo sequences were used.

4. DISCUSSION

The decoherence of the spin-echo signal, given by the envelope $F(\tau)$ in Figure 2a, is caused by magnetic dipole-dipole interactions between ^{13}C nuclear spins. As a result, the achievable sensitivity might vary from center to center since each defect has different local distribution of nuclei spins. This decoherence or envelope was modeled with an exponential decay modulated by the effect of a pair of nearby strongly interacting ^{13}C. In this model,[23] $F(\tau) = \exp(-(\tau/T_2)^4)(1 - \frac{(a^2-b^2)}{a^2}\sin^2 a\tau \sin^2 b\tau)$; where for the data in Figure 2a we found $T_2 = 676$ μs, $b = 478$ Hz (corresponding to the dipolar interaction between the two nuclei) and $a = 626$ Hz (related with the interactions between the nuclei and the NV spin).

The absolute sensitivity depends on the signal to noise ratio in the readout of the NV electronic spin state. In our case, this is limited by photon collection efficiency $\approx 0.1\%$. The resulting photon shot noise[7,16] results in a degradation of the ideal magnetometer sensitivity given by[16] $\eta_{AC} = \frac{\pi\hbar}{g\mu_B C\sqrt{\nu F(1/\nu)}}$. The solid curve in Figure 3-a is the predicted sensitivity η_{AC} as a function of the frequency of the external magnetic field where $g \approx 2$ is the electron g-factor, μ_B is the Bohr magneton, and $C^{-1} = \sqrt{1 + 2\frac{(a_0+a_1+a_0a_1)}{(a_0-a_1)^2}}$ is a factor that estimates[16] the photon shot-noise when the average photon number during the readout window of 324 ns is much less than 1. The values $a_0 = 0.03 \pm 0.006$ and $a_1 = 0.018 \pm 0.004$ correspond to the average number of detected photons for the electronic spin states $m_S = 0$ and $m_S = \pm 1$, respectively. This prediction is in excellent agreement with the experimental results, indicating that our magnetometer is photon-shot-noise limited.

5. OUTLOOK

The present achieved sensitivity and high spatial resolution suggest that solid state spin-qubits such as NV centers in diamond can find a wide range of applications, from fundamental physics tests or quantum computing applications to detection of NMR signals, surface physics and material science, and medical imaging and biomagnetism. In particular, this robust technology could be invaluable both in nanoscale magnetic field imaging and in macroscopic field detection scenarios, such as low-field MRI.

For instance, one of the outstanding challenges in magnetic sensing is the detection and real space imaging of single electronic and nuclear dipoles. Since the magnetic field from a single dipole decreases with distance as $\sim 1/r^3$, a magnetometer that can be brought into close proximity of the dipole offers a clear advantage. This can be achieved by using a diamond nanocrystal. For example, a ~ 25 nm diameter nanocrystal attached to the end of an optical fiber or plasmonic waveguide,[25] would provide a spatial resolution ~ 25 nm, while achieving orders of magnitude higher magnetic field sensitivity than magnetic force microscopy.[12] Provided the waveguide can yield high collection efficiency ($C \gtrsim 0.3$), a sensitivity better than 3 nT $\mathrm{Hz}^{-1/2}$ could be achieved using echo-based techniques. This surpasses the sensitivity of Hall-bar[26] or SQUID[8] based microscopes by more than an order of magnitude, with 10 times better spatial resolution. For example, the magnetic field from a single proton is ~ 3 nT at 10-nm separation, which an NV nanocrystal magnetometer would be able to detect within one second. The ultimate limits to miniaturization of such nanocrystals, which are likely due to surface effects, are not yet well understood, but experiments have already demonstrated control of single NV centers in sub 50-nm nanocrystals,[24, 27, 28] as well as the use of such nanocrystals in scanning probe setups.[29]

The magnetic field sensitivity can be improved further by using multiple pulses. The narrow bandwidth associated with such an approach can also be exploited for a frequency selective measurement, ranging from tens of kHz up to MHz. This will enable to distinguish different isotopes, due to their unique gyromagnetic ratios, and could improve the spatial resolution when used in combination with a strong magnetic field gradient. Much longer coherence and interrogation times should be possible by using isotopically pure diamond with low concentrations of both ^{13}C and nitrogen electron spin impurities. The signal-to-noise ratio may also be increased by improving the measurement readout efficiency. Near single-shot readout of an electronic spin in diamond has been achieved with cryogenic cooling using resonant excitation.[30] Photon collection efficiency at room temperature can also be substantially improved using either conventional far-field optics or evanescent, near-field coupling to optical waveguides.[31] Finally, another way to improve the magnetometer sensitivity is to use many sensing spins,[16] where we can take advantage of the relatively high achievable density of spins in the solid-state ($\sim 10^{17}$ cm^{-3}) compared to atomic magnetometers($\sim 10^{13}$ cm^{-3}).[7] Further extensions could include the use of non-classical spin states, such as squeezed states induced by the spin-spin coupling.

The above considerations indicate that coherent control of electronic spins in diamond can be used to create a magnetic field sensor with an unprecedented combination of sensitivity and spatial resolution in a small, robust device. On a more general level, these ideas could apply to a variety of paramagnetic systems or even qubits sensitive to other perturbations of their environment. The vast range of potential applications for sensitive, spatially resolved measurements warrants a re-examination of solid-state quantum devices from the perspective of metrology.

Acknowledgments

We gratefully acknowledge conversations with D. Awschalom, A. Cohen, J. Doyle, D. Budker and M. P. Ledbetter. This work was supported by the NSF, DARPA, MURI and David and Lucile Packard Foundation.

REFERENCES

1. D. Budker, D. F. Kimball, and D. P. DeMille, *Atomic Physics: An Exploration Through Problems and Solutions*, Oxford University Press, 2004.
2. N. F. Ramsey, *Molecular Beams*, Oxford University Press, 1990.

3. A. D. Ludlow, T. Zelevinsky, G. K. Campbell, S. Blatt, M. M. Boyd, M. H. G. de Miranda, M. J. Martin, J. W. Thomsen, S. M. Foreman, J. Ye, T. M. Fortier, J. E. Stalnaker, S. A. Diddams, Y. Le Coq, Z. W. Barber, N. Poli, N. D. Lemke, K. M. Beck, and C. W. Oates, "Sr Lattice Clock at 1 x 10-16 Fractional Uncertainty by Remote Optical Evaluation with a Ca Clock," *Science* **319**(5871), pp. 1805–1808, 2008.
4. T. Rosenband, D. B. Hume, P. O. Schmidt, C. W. Chou, A. Brusch, L. Lorini, W. H. Oskay, R. E. Drullinger, T. M. Fortier, J. E. Stalnaker, S. A. Diddams, W. C. Swann, N. R. Newbury, W. M. Itano, D. J. Wineland, and J. C. Bergquist, "Frequency ratio of Al^+ and Hg^+ single-ion optical clocks; metrology at the 17th decimal place," *Science* **319**(5871), pp. 1808–1812, 2008.
5. D. J. Wineland, J. J. Bollinger, W. M. Itano, F. L. Moore, and D. J. Heinzen, "Spin squeezing and reduced quantum noise in spectroscopy," *Phys. Rev. A* **46**(11), p. R6797, 1992.
6. I. K. Kominis, T. W. Kornack, J. C. Allred, and M. V. Romalis, "A subfemtotesla multichannel atomic magnetometer," *Nature* **422**(6932), pp. 596–599, 2003.
7. D. Budker and M. Romalis, "Optical magnetometry," *Nat Phys* **3**(4), pp. 227–234, 2007.
8. S. J. Bending, "Local magnetic probes of superconductors," *Advances in Physics* **48**(4), p. 449, 1999.
9. R. Kleiner, D. Koelle, F. Ludwig, and J. Clarke, "Superconducting quantum interference devices: State of the art and applications," *Proc. of the IEEE* **92**(10), pp. 1534–1548, 2004.
10. C. N. Owston, "A hall effect magnetometer for small magnetic fields," *J. Sci. Instrum.* **44**(9), pp. 798–800, 1967.
11. D. Rugar, R. Budakian, H. J. Mamin, and B. W. Chui, "Single spin detection by magnetic resonance force microscopy," *Nature* **430**(6997), pp. 329–332, 2004.
12. H. J. Mamin, M. Poggio, C. L. Degen, and D. Rugar, "Nuclear magnetic resonance imaging with 90-nm resolution," *Nature Nano* **2**(5), pp. 301–306, 2007.
13. F. Jelezko, T. Gaebel, I. Popa, A. Gruber, and J. Wrachtrup, "Observation of coherent oscillations in a single electron spin," *Phys. Rev. Lett.* **92**(7), p. 076401, 2004.
14. F. Jelezko, T. Gaebel, I. Popa, M. Domhan, A. Gruber, and J. Wrachtrup, "Observation of coherent oscillation of a single nuclear spin and realization of a two-qubit conditional quantum gate," *Phys. Rev. Lett.* **93**, p. 130501, Sep 2004.
15. L. Childress, M. V. Gurudev Dutt, J. M. Taylor, A. S. Zibrov, F. Jelezko, J. Wrachtrup, P. R. Hemmer, and M. D. Lukin, "Coherent dynamics of coupled electron and nuclear spin qubits in diamond," *Science* **314**(5797), pp. 281–285, 2006.
16. J. M. Taylor, P. Cappellaro, L. Childress, L. Jiang, D. Budker, P. R. Hemmer, A. Yacoby, Walsworth, and M. D. Lukin, "High-sensitivity diamond magnetometer with nanoscale resolution," *Nat Phys* **4**(10), pp. 810–816, 2008.
17. J. R. Maze, P. L. Stanwix, J. S. Hodges, S. Hong, J. M. Taylor, P. Cappellaro, L. Jiang, M. V. G. Dutt, E. Togan, A. S. Zibrov, A. Yacoby, R. L. Walsworth, and M. D. Lukin, "Nanoscale magnetic sensing with an individual electronic spin in diamond," *Nature* **455**(7213), pp. 644–647, 2008.
18. G. Balasubramanian, I. Y. Chan, R. Kolesov, M. Al-Hmoud, J. Tisler, C. Shin, C. Kim, A. Wojcik, P. R. Hemmer, A. Krueger, T. Hanke, A. Leitenstorfer, R. Bratschitsch, F. Jelezko, and J. Wrachtrup, "Nanoscale imaging magnetometry with diamond spins under ambient conditions," *Nature* **455**(7213), pp. 648–651, 2008.
19. E. L. Hahn, "Spin echoes," *Phys. Rev.* **80**, pp. 580–594, Nov 1950.
20. S. Meiboom and D. Gill, "Modified spin-echo method for measuring nuclear relaxation times," *Rev. Sc. Instr.* **29**(8), pp. 688–691, 1958.
21. G. R. Khutsishvili, "Spin diffusion," *Sov. Phys. Uspekhi* **8**(5), pp. 743–769, 1966.
22. M. V. G. Dutt, L. Childress, L. Jiang, E. Togan, J. Maze, F. Jelezko, A. S. Zibrov, P. R. Hemmer, and M. D. Lukin, "Quantum register based on individual electronic and nuclear spin qubits in diamond," *Science* **316**(5829), pp. 1312–1316, 2007.
23. J. R. Maze, J. M. Taylor, and M. D. Lukin, "Electron spin decoherence of single nitrogen-vacancy defects in diamond," *Phys. rev. B* **78**(9), p. 094303, 2008.
24. J. R. Rabeau, A. Stacey, A. Rabeau, S. Prawer, F. Jelezko, I. Mirza, and J. Wrachtrup, "Single nitrogen vacancy centers in chemical vapor deposited diamond nanocrystals," *Nano Lett.* **7**(11), pp. 3433–3437, 2007.

25. D. E. Chang, A. S. Sorensen, E. A. Demler, and M. D. Lukin, "A single-photon transistor using nanoscale surface plasmons," *Nat Phys* **3**(11), pp. 807–812, 2006.
26. A. M. Chang, H. D. Hallen, L. Harriott, H. F. Hess, H. L. Kao, J. Kwo, R. E. Miller, R. Wolfe, J. van der Ziel, and T. Y. Chang, "Scanning hall probe microscopy," *Appl. Phys. Lett.* **61**(16), pp. 1974–1976, 1992.
27. T. Gaebel, M. Domhan, I. Popa, C. Wittmann, P. Neumann, F. Jelezko, J. R. Rabeau, N. Stavrias, A. D. Greentree, S. Prawer, J. Meijer, J. Twamley, P. R. Hemmer, and J. Wrachtrup, "Room-temperature coherent coupling of single spins in diamond," *Nat Phys* **2**(6), pp. 408–413, 2006.
28. J. R. Rabeau, P. Reichart, G. Tamanyan, D. N. Jamieson, S. Prawer, F. Jelezko, T. Gaebel, I. Popa, M. Domhan, and J. Wrachtrup, "Implantation of labelled single nitrogen vacancy centers in diamond using ^{15}N," *Appl. Phys. Lett.* **88**(2), p. 023113, 2006.
29. S. Khn, C. Hettich, C. Schmitt, J.-P. Poizat, and V. Sandoghdar, "Diamond colour centres as a nanoscopic light source for scanning near?field optical microscopy," *J. Microsc.* **202**(1), pp. 2–6, 2001.
30. J. Wrachtrup and F. Jelezko, "Processing quantum information in diamond," *J. Phys. Cond. Matt.* **18**(21), pp. S807–S824, 2006.
31. D. E. Chang, A. S. Sorensen, P. R. Hemmer, and M. D. Lukin, "Quantum optics with surface plasmons," *Phys. Rev. Lett.* **97**(5), p. 053002, 2006.